Title
Anisotropic Formation and Distribution of Stacking Faults in II–VI Semiconductor Nanorods

Journal
Nano Letters, 13(1)

ISSN
1530-6984

Authors
Hughes, Steven M.
Alivisatos, A. Paul

Publication Date
2013-01-09

NANO LETTERS

Letter

pubs.acs.org/NanoLett

Anisotropic Formation and Distribution of Stacking Faults in II–VI Semiconductor Nanorods

Steven M. Hughes*,† and A. Paul Alivisatos

Department of Chemistry, University of California, Berkeley, California 94720, United States

Material Science Division, Lawrence Berkeley National Laboratory, Berkeley, California 94720, United States

Supporting Information

ABSTRACT: Nanocrystals of cadmium selenide exhibit a form of polytypism with stable forms in both the wurtzite and zinc blende crystal structures. As a result, wurtzite nanorods of cadmium selenide tend to form stacking faults of zinc blende along the *c*-axis. These faults were found to preferentially form during the growth of the (001) face, which accounts for 40% of the rod's total length. Since II–VI semiconductor nanorods lack inversion symmetry along the *c*-axis of the particle, the two ends of the nanorod may be identified by this anisotropic distribution of faults.

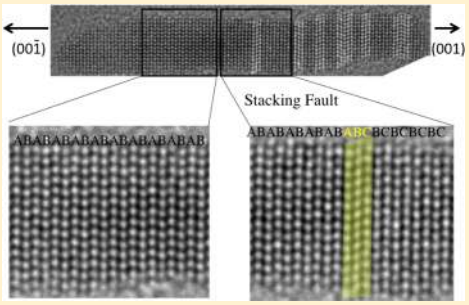

KEYWORDS: *Nanocrystal, nanorod, stacking fault, CdSe, orientation, heterostructure*

Nanomaterials are assuming an important role in emerging technologies. In many of these applications, two of the most desired properties are reproducibility and uniformity of high quality materials. In order to attain this goal though, first one must understand how defects arise, which can detract from a material's quality, in order to find new methods to avoid them in the future. Some of the most well-developed materials are the cadmium based II–VI semiconductor nanocrystals. With established synthetic methods for the formation of dots,[1,2] rods,[3−5] tetrapods,[6] as well as branched heterostructures,[7] these systems have been thoroughly studied for many applications from light emitting diodes[8−10] to solar cells,[11−13] and single electron transistors.[14,15]

These II–VI chalcogenides display a form of polytypism with stable forms in both the hexagonal wurtzite and cubic zinc blende.[16,17] The two crystal packings, and the ability to form both under typical nanoparticle growth conditions, are the source of the advanced shape control. While the cubic form is chemically isotropic, growing as a tetrahedral structure with four equivalent faces, the wurtzite form is more complex. Growth of the wurtzite structure leads to the formation of a nanorod with the majority of the crystal growth occurring along the *c*-axis.[3,18] Because the faces at either end of the rod are chemically different, there is no inversion symmetry along this axis. If unreconstructed and not ligated, the cadmium atoms on the (001) face would have a single dangling bond, while the cadmium atoms on the (00$\bar{1}$) face would have three dangling bonds. Due to this anisotropy, the (001) face is commonly referred to as the slow growing face, while the (00$\bar{1}$) is considered the fast growing face and likely the source for the majority of the rod's growth. This anisotropic structure also leads to a net dipole in the rod, which has been a source of great interest and research.[19−21]

Unfortunately, it is this same polytypism that leads to the formation of stacking faults in the nanorods. The [001] faces of wurtzite are indistinguishable from and match up with the [111] faces of zinc blende.[6] Therefore, stacking faults arise when a certain number of zinc blende (ABCABC) layers form during growth within the greater wurtzite (ABAB) lattice. A complex fault (ABABCBC) is the most commonly observed fault with three layers of zinc blende. In an intrinsic fault (ABABCACA), there are four zinc blende layers, and in an extrinsic fault (ABABCABAB) there are five.[22] When properly oriented, each of these patterns can be directly observed for individual nanorods using high-resolution transmission electron microscopy (HRTEM).

Only by truly understanding how these nanomaterials grow can we hope to improve them and subsequently integrate them into more complex systems and advanced devices. In this Letter, we present a careful, detailed analysis of the formation of stacking faults based on a statistical description of their position within individual nanorods. We consider the fault distribution in both rods of varying aspect ratios, as well as their formation over time, in order to develop a more complete picture of nanorod growth. While stacking faults have not been shown to directly effect optical properties such as photoluminescence quantum yield, they do change the surface of the nanorod, which can result in poorer surface passivation and inconsistencies with subsequent growth such as shelling. An improved understanding of their growth will allow future researchers to synthesize more monodisperse particles with

Received: September 30, 2012
Revised: December 14, 2012
Published: December 19, 2012

fewer stacking faults for greater uniformity and superior passivation. Additionally, using this newfound understanding of fault formation, we present a method whereby stacking faults are used as an internal standard for detecting the orientation of a single nanorod both alone as well as in more complex systems. Because of the nanorod's net dipole, there is a great interest in understanding how the particles are aligned; unfortunately it can be a daunting task to actually determine this orientation.[23] Since stacking faults arise naturally in these nanorods, using them as an internal standard provides a convenient method to solve a challenging problem.

Stacking Fault Distribution. For the purpose of this study, unless otherwise noted, CdSe rods were grown by the previously reported synthetic method based on a CdO precursor complexed with alkylphosphonic acids.[7] Previous belief held that faults were formed randomly within the rod in which case there should be no observable pattern in their location. However, a clearly anisotropic distribution of the faults along the length of the rods was observed in this study, as shown in Figure 1. While the number of faults and their exact

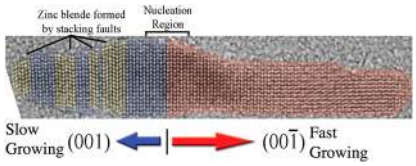

Figure 1. The above model for rod growth has the rod split into two regions of growth after an initial nucleation event. The growth from the (00$\bar{1}$) face is fast and mostly fault free. The growth in the opposite direction from the (001) face is slower and highly faulted. The faults in the slow growing region have been highlighted in yellow.

locations change for each individual rod, the region in which they formed remained a fixed percent of the rods overall length (Figure 2). In the case of the three sets of rods of varying length shown here, that region makes up approximately 40% of the rod. Consequently, the rod may be characterized as having two different regions, one accounting for this area of high fault

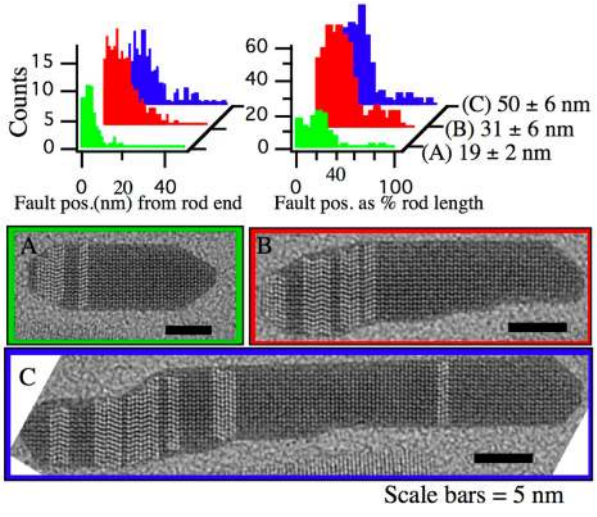

Figure 2. Statistics taken from 19 (A), 31 (B), and 50 nm (C) rods. Left plot contains histograms of actual stacking fault positions as measured from the end of the rod with higher fault density. The right plot contains histograms with the same fault position data only normalized as a percent of the individual rod lengths.

density, while the other part of the rod is mostly fault free. Allowing that the nanorod formation is a kineticly driven process,[24,25] these two regions then account for two different growth regimes. By inference, the smaller region containing the faults can be attributed to the slow growing (001) face, while the larger fault free region is thus due to the fast growing (00$\bar{1}$) face, Figure 1. These observations are in agreement with recent studies of seeded nanorod growth. In these complementary experiments, one end of the rod was found to grow 2−3 times faster than the other off the ends of the seed particle.[17,26−28]

This regional growth is dependent solely on the growth rates of the two [001] faces and not the actual time of growth or overall size of rod. This can be seen clearly in a rod that is analyzed at multiple points in time throughout its growth, Figure 3. During the progression of growth shown here the rod

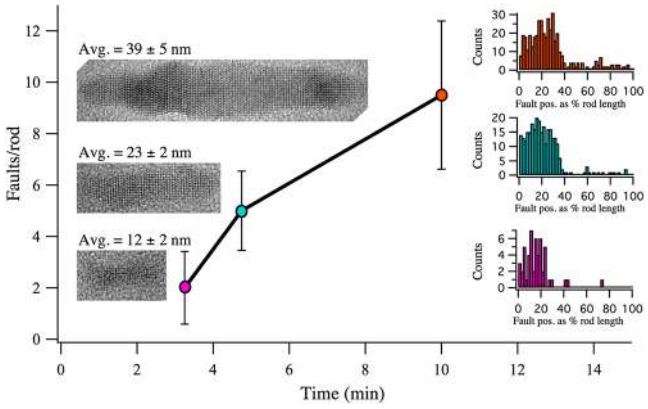

Figure 3. In the single growth experiment above, as the rods mature more faults continue to form. Aliquots were taken and characterized at 12, 23, and 39 nm. At 12 nm, there is an average of 2 faults/rod, at 23 nm there are 5 faults/rod, and finally at 39 nm there are 9 faults/rod. Additionally, the shape of the distribution of faults in the rods remains consistent as shown in the histograms on the right.

grows from 14.8 ± 1.7 nm sampled at 3:15 min, to 23.7 ± 2.4 nm at 4:45 min, and ending at 42.9 nm ± 4.3 nm after 10:00 min. As the growth continues the data shows that faults continue to form as well throughout the synthesis, increasing from an average of 2 faults/rod to 4 faults/rod, and ending at approximately 10 faults/rod. After an initial increase between the first two sampled periods, the distribution appears to stabilize at a 40/60 split between the growth regions. For this distribution to be maintained throughout the growth, the faults must continue to form throughout the rod's growth at a fixed rate as well as on a particular end.

Changes in the rod's kinetics and the ratio of the growth rates between the (001) and (00$\bar{1}$) faces will change the relative size of the fault region, and therefore affect the quality of the resulting sample. Thus by decreasing the size of this fault region, more defect free rods may be grown. This has been observed in the comparison of rods grown by the forementioned technique using cadmium oxide as the precursor versus rods grown using a previously published technique using dimethyl cadmium as the cadmium precursor.[29] The rods grown using this preparatory technique tend to be of a higher quality (fewer faults) and of a higher aspect ratio. For example, in a sample of 29 × 6 nm rods there is an average of 3 faults/rod, which are in a region accounting for only 20% of the rod's length. Compared with the 9 faults/rod for the 31 nm long rods in Figure 2, one can see why it may be that these rods are often

dx.doi.org/10.1021/nl3036417 | Nano Lett. 2013, 13, 106−110

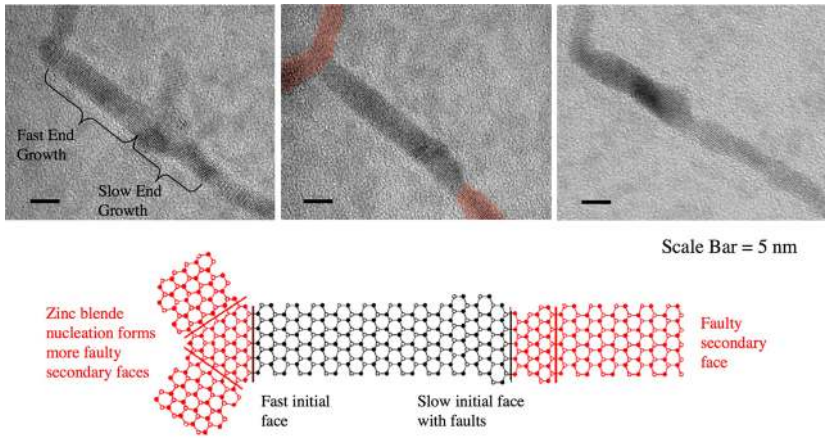

Figure 4. HRTEM and stick model of CdSe/CdTe heterostructures formed by seeding CdTe growth with a CdSe nanorod. The faulty linear CdTe growth extends from the slow growing (001) face of the CdSe nanorod, while the zinc blende nucleation and subsequent branching occurs on the fast growing $(00\bar{1})$ face of the CdSe.

preferred for experiments that require a higher quality sample such as alignment in liquid crystals.

This anisotropic distribution, though, does not appear to be isolated to CdSe. Cadmium sulfide rods grown by a similar method[7] exhibit this behavior as well. For a 29.1 ± 4.1 nm rod, an average of 3 faults/rod was found confined in a region of approximately 20% of the rod's length. This result suggests that the anisotropic fault distribution may be a more generalized phenomenon that may be observed in other II/VI semiconductor nanomaterials as well as those observed in this study.

These results point to two conclusions regarding the formation of stacking faults in CdSe nanorods. First, given the location and distribution of faults in the nanorod, along with their constant rate of formation, it is evident that the faults form during the growth off the slow growing (001) face. Therefore, by identifying the end of the rod with the greater number density of stacking faults, one may infer the orientation of the crystal and inherent dipole. Second, as the faults are formed by the growth from the slow growing face, it is clear that like the rod itself their formation is a kinetically driven process. Thermodynamics would suggest that faults would form preferentially in the region grown by the higher energy $(00\bar{1})$ face. This growth, which represents approximately 60% of the rods studied here, is highly uniform and largely fault free. Thus, by controlling the kinetics of the nanorod growth, one may potentially tune the quality and uniformity of the rods by limiting the growth of the (001) face and subsequently the fault formation as well.

These results do raise into question the use of "slow" and "fast" growing to describe the (001) and $(00\bar{1})$ faces, respectively. The 40/60 split of the final nanorod indicates that in these particles the $(00\bar{1})$ face was growing only 1.5 times faster than the (001) face. However, since the goal of most researchers will be to decrease the contribution of the faulty (001) face, the growth rate of that surface will likely become even slower. Thus, the nomenclature of "slow" and "fast" to describe the two crystal faces appears to still be relevant.

Finally, the relative growth rates of the two faces in a kinetically driven process will depend on the relative energies of the two surfaces in solution, and subsequently the activation energy of growing new material on each crystal face. While it is beyond the scope of this work, to predictively control the relative growth rates of the (001) and $(00\bar{1})$ faces in the future a study of the ligand passivation present during growth would be greatly beneficial. Because the two surfaces are chemically different, one must consider both the strength of the ligand binding to the available atoms and the sterics of the surface coverage. Because of the nature of these chemical reactions, this is an extraordinarily complex problem given the variety of active reagents and byproducts formed during a typical nanocrystal synthesis. The results of this work, though, would suggest that the energies of the two faces are in fact not as different as previously believed.

Characterization of Complex Systems. By qualitatively extending these results to more complex systems, it becomes clear how the stacking faults may be used as internal standards for orientation. As an example system, consider the CdSe/CdTe heterostructures as shown in Figure 4. These structures first reported by Milliron et al. are grown by seeding CdTe growth using CdSe nanorods.[7] The structures are characterized by the preferential growth of a linear extension off one end of the initial rod (lower right of Figure 4 images), while the other end nucleates a region of zinc blende that leads to branching arms of CdTe (upper left). It is clear that the chemistry of the nanorod's two end faces leads to the different behavior of the CdTe as it is introduced to the system.

By visual inspection of the HRTEM images, it can be seen that one end of the initial nanorod contains a greater density of stacking faults. This may be observed both by a careful analysis of the fault location as well as by the irregular bulging shape at one end of the rod that arises due to the presence of the stacking faults. This end of the rod may therefore be attributed to the growth of the (001) face. From this characterization, it is clear that the linear CdTe growth occurs on the slow growing (001) face of the initial CdSe rod, whereas the zinc blende nucleation and subsequent branching occurs on the fast growing $(00\bar{1})$ face. This growth mechanism explains the overall faultiness of these particles. The zinc blende nucleation on the fast growing face will result in the formation of additional slow growing, fault-rich faces as new arms are grown off the branch point.

As a second example of the utility of this internal measure, consider the process of nucleating gold particles on a CdSe nanorod.[30−32] When performed very carefully it has been observed that the nucleation of the gold begins on the ends of the rods. This makes sense as these regions offer higher energy

dx.doi.org/10.1021/nl3036417 | Nano Lett. 2013, 13, 106−110

surfaces for the metal deposition. When slowed sufficiently, one can stop the process when only a single end of the rod has been tipped (Figure 5). Initial observations of these particles suggest

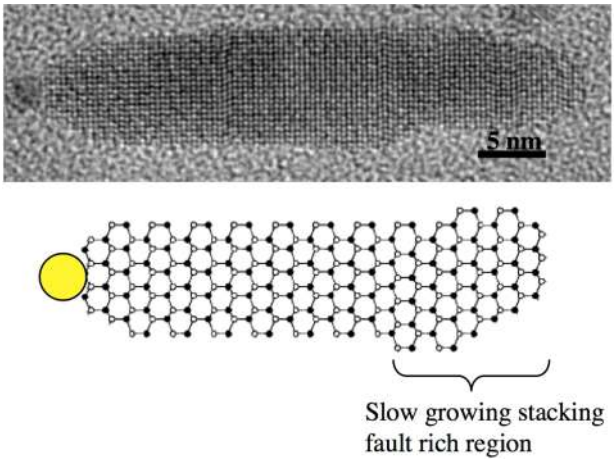

Figure 5. HRTEM and stick model of selective gold deposition on the end of a CdSe nanorod. As shown here, the gold appears to preferentially form on the fast growing $(00\bar{1})$ face of the nanorod.

that as one might expect, initial gold deposition appears to happen on the higher energy surface of the fast growing $(00\bar{1})$ face. Again, this conclusion is based on identifying the region of the rod with the greater density of stacking faults. In Figure 5, one can observe the region on the right has far more faults than that of the left end of the particle. The (001) face, is therefore on the right side, and the $(00\bar{1})$ is on the left. From the HRTEM image, one can see the clearly formed gold bead on the $(00\bar{1})$ face, while the (001) face is still bare.

These findings give new insight to the growth mechanism of nanocrystals as well as convenient new tool for characterization of complex structures. The results suggest that the slow growing face is in fact not considerably slower growing and contributes more to the size and quality of the rod than previously thought. More importantly, the degree of this contribution may be controlled to form higher quality rods by altering the synthetic technique to limit the role of the slow growing crystal face during growth. By limiting the growth of this face, researchers should be able to grow more monodisperse nanorods with greater consistency and improved passivation due to surface uniformity. Additionally, since the faults appear to be preferentially grown on the slow growing face, the orientation of the rod may be identified by identifying the region of greater fault density. This region in turn corresponds to the end of the rod formed by the slow growing (001) face. As we demonstrated here, this is an extraordinarily useful tool when characterizing more complex systems.

Experimental Conditions. Typical rod growth was performed using cadmium oxide complexed with alkylphosphonic acids for the cadmium precursor under air free conditions. The cadmium oxide was mixed in a roughly 1:2 (Cd/phosphonic acids) ratio with phosphonic acids (75% tetradecylphosphonic acid and 25% hexylphosphonic acid) and disolved in trioctyl-phosphine oxide (TOPO) at 120 °C. The CdO dissociates around 200 °C and the anion precursor, complexed with trioctyl-phosphine (TOP), was injected at roughly 300 °C. The rods were grown for approximately 5 −10 min (depending on desired size) after anion injection. Using slight modifications of this general procedure, CdSe rods were grown with the following dimensions (nm): 49.5 ± 6.2 nm × 6.4 ± 0.7 nm, 31.4 ± 5.8 × 6.2 ± 0.6 nm, 18.7 ± 2.2 nm × 7.0 ± 0.7 nm, and a single synthesis of rods sampled at multiple times of 12.0 ± 2.2 nm (3:15 min), 23.3 ± 2.3 nm (4:45 min), and 39.3 ± 5.0 nm (10:00 min). The average number of faults per rod ranged from 2 for the 12.0 nm long rods to 10 for the 39.3 nm long rods. Cadmium sulfide rods, grown in a similar fashion, were 29.1 ± 4.1 nm long. Finally, CdSe rods grown using dimethylcadmium precursor, a common used technique, were grown to 21.2 ± 2.4 nm long.

HRTEM was performed using a 200 kV LaB_6 FEI Tecnai G^2 20, equipped with a Super TWIN lens. The number and location of each stacking pattern was recorded for approximately 60 nanorods from each sample, and measurements were recorded with respect to the end with the highest density of faults for consistency.

■ ASSOCIATED CONTENT

Ⓢ Supporting Information

Figures highlighting the analysis of CdSe/CdTe heterostructures, CdSe nanorods grown with dimethylcadmium, and gold-tipped CdSe nanorods. This material is available free of charge via the Internet at http://pubs.acs.org.

■ AUTHOR INFORMATION

Corresponding Author

*E-mail: hughess2@whitman.edu.

Present Address

[†]Chemistry Department, Whitman College, Walla Walla, Washington 99362, United States.

Notes

The authors declare no competing financial interest.

■ ACKNOWLEDGMENTS

The authors of this work would like to extend their thanks to H. Liu, B. Sadtler, D. Milliron, A. Mastroianni, P. Trudeau, and J. Owen for their indispensable conversations and constructive feedback throughout the development of this work. Part of the TEM work presented here was performed with a user grant at the National Center of Electron Microscopy (NCEM), which is funded by the Director, Office of Science, Office of Basic Energy Sciences, of the United States Department of Energy under contract DE-AC02-05CH11231. Work on stacking fault characterization by Steven Hughes and A. P. Alivisatos was supported by the Director, Office of Science, Office of Basic Energy Sciences, of the United States Department of Energy under contract DE-AC02-05CH11231.

■ REFERENCES

(1) Norris, D.; Bawendi, M. *Phys. Rev. B: Condens. Matter* **1996**, *53*, 16338−16346.

(2) Kundu, J.; Ghosh, Y.; Dennis, A. M.; Htoon, H.; Hollingsworth, J. A. *Nano Lett.* **2012**, *12* (6), 3031−3037.

(3) Manna, L.; Scher, E.; Alivisatos, A. *J. Am. Chem. Soc.* **2000**, *122*, 12700−12706.

(4) Talapin, D. V.; Mekis, I.; Götzinger, S.; Kornowski, A.; Benson, O.; Weller, H. *J. Phys. Chem. B* **2004**, *108*, 18826−18831.

(5) Deka, S.; Quarta, A.; Lupo, M. G.; Falqui, A.; Boninelli, S.; Giannini, C.; Morello, G.; De Giorgi, M.; Lanzani, G.; Spinella, C.; Cingolani, R.; Pellegrino, T.; Manna, L. *J. Am. Chem. Soc.* **2009**, *131*, 2948−2958.

(6) Manna, L.; Milliron, D. J.; Meisel, A.; Scher, E. C.; Alivisatos, A. P. *Nat. Mater.* **2003**, *2*, 382−385.

(7) Milliron, D. J.; Hughes, S. M.; Cui, Y.; Manna, L.; Li, J.; Wang, L.-W.; Alivisatos, A. P. *Nature* **2004**, *430*, 190−195.
(8) Pal, B. N.; Ghosh, Y.; Brovelli, S.; Laocharoensuk, R.; Klimov, V. I.; Hollingsworth, J. A.; Htoon, H. *Nano Lett.* **2012**, *12*, 331−336.
(9) Bae, W. K.; Kwak, J.; Lim, J.; Lee, D.; Nam, M. K.; Char, K.; Lee, C.; Lee, S. *Nano Lett.* **2010**, *10*, 2368−2373.
(10) Rogach, A. L.; Gaponik, N.; Lupton, J. M.; Bertoni, C.; Gallardo, D. E.; Dunn, S.; Li Pira, N.; Paderi, M.; Repetto, P.; Romanov, S. G.; O'Dwyer, C.; Sotomayor Torres, C. M.; Eychmüller, A. *Angew. Chem., Int. Ed.* **2008**, *47*, 6538−6549.
(11) Milliron, D. J.; Gur, I.; Alivisatos, A. P. *MRS Bull.* **2005**, *30*, 41−44.
(12) Schierhorn, M.; Boettcher, S. W.; Kraemer, S.; Stucky, G. D.; Moskovits, M. *Nano Lett.* **2009**, *9*, 3262−3267.
(13) Bang, J. H.; Kamat, P. V. *ACS Nano* **2009**, *3*, 1467−1476.
(14) Klein, D.; Roth, R.; Lim, A.; Alivisatos, A.; McEuen, P. *Nature* **1997**, *389*, 699−701.
(15) Cui, Y.; Banin, U.; Björk, M. T.; Alivisatos, A. P. *Nano Lett.* **2005**, *5*, 1519−1523.
(16) Yeh, C.; Lu, Z.; Froyen, S.; Zunger, A. *Phys. Rev. B: Condens. Matter* **1992**, *46*, 10086−10097.
(17) Huang, J.; Kovalenko, M. V.; Talapin, D. V. *J. Am. Chem. Soc.* **2010**, *132*, 15866−15868.
(18) Peng, X.; Manna, L.; Yang, W.; Wickham, J.; Scher, E.; Kadavanich, A.; Alivisatos, A. *Nature* **2000**, *404*, 59−61.
(19) Luo, Y.; Wang, L.-W. *ACS Nano* **2010**, *4*, 91−98.
(20) Singh, A.; Gunning, R. D.; Sanyal, A.; Ryan, K. M. *Chem. Commun.* **2010**, *46*, 7193−7195.
(21) Li, L.-S.; Alivisatos, A. *Phys. Rev. Lett.* **2003**, *90*, 097402.
(22) Takeuchi, S.; Suzuki, K.; Maeda, K.; Iwanaga, H. *Philos. Mag. A* **1985**, *50*, 171−178.
(23) Bertoni, G.; Grillo, V.; Brescia, R.; Ke, X.; Bals, S.; Catellani, A.; Li, H.; Manna, L. *ACS Nano* **2012**, *6*, 6453−6461.
(24) Bullen, C. R.; Mulvaney, P. *Nano Lett.* **2004**, *4*, 2303−2307.
(25) Owen, J. S.; Chan, E. M.; Liu, H.; Alivisatos, A. P. *J. Am. Chem. Soc.* **2010**, *132*, 18206−18213.
(26) Talapin, D. V.; Nelson, J. H.; Shevchenko, E. V.; Aloni, S.; Sadtler, B.; Alivisatos, A. P. *Nano Lett.* **2007**, *7*, 2951−2959.
(27) Dorfs, D.; Salant, A.; Popov, I.; Banin, U. *Small* **2008**, *4*, 1319−1323.
(28) Choi, C. L.; Koski, K. J.; Sivasankar, S.; Alivisatos, A. P. *Nano Lett.* **2009**, *9*, 3544−3549.
(29) Manna, L.; Scher, E. C.; Li, L.-S.; Alivisatos, A. P. *J. Am. Chem. Soc.* **2002**, *124*, 7136−7145.
(30) Figuerola, A.; Huis, M. V.; Zanella, M.; Genovese, A.; Marras, S.; Falqui, A.; Zandbergen, H. W.; Cingolani, R.; Manna, L. *Nano Lett.* **2010**, *10*, 3028−3036.
(31) Salant, A.; Amitay-Sadovsky, E.; Banin, U. *J. Am. Chem. Soc.* **2006**, *128*, 10006−10007.
(32) Mokari, T.; Rothenberg, E.; Popov, I.; Costi, R.; Banin, U. *Science* **2004**, *304*, 1787−1790.

dx.doi.org/10.1021/nl3036417 | *Nano Lett.* 2013, 13, 106−110